PAPER NO. 85-3550

REAL-TIME VISION-SERVOING OF A ROBOTIC TREE FRUIT HARVESTER

by

R. C. Harrell, P. D. Adsit, and D. C. Slaughter
Assistant Professor, Graduate Student[2]
Department of Agricultural Engineering
University of Florida
Gainesville, Florida

For presentation at the 1985 Winter Meeting
AMERICAN SOCIETY OF AGRICULTURAL ENGINEERS

Hyatt Regency, Chicago IL
December 17-20, 1985

SUMMARY:

Vision-servo control loops for a tree fruit harvesting robot were developed and analyzed. Closed form solutions for vision gains were developed. A comparision of vision-servo loop dynamics when utilizing proportional and proportional plus derivative control is presented.

American Society of Agricultural Engineers

St. Joseph, MI 49085-9659

REAL-TIME VISION-SERVOING OF A ROBOTIC TREE FRUIT HARVESTER

R.C. Harrell, P.D. Adsit, and D.C. Slaughter
Department of Agricultural Engineering
University of Florida

Tree fruit harvesting is an agricultural operation which has yet to experience widespread mechanization. Attempts at harvesting using mechanical shakers or oscillating blasts of air have been only partially successful. Harvesting is still dependent on a large seasonal workforce and accounts for more than 20% of the price growers receive for their products [1]. Recent advances in robotics and related sensor technologies make possible a completely new approach for harvesting tree fruit crops. Machine vision offers a method to identify and locate ripe fruit on the tree. Variations of present industrial manipulators equipped with specially designed end-effectors can be used to pick targeted fruit. However, to develop robotic systems that can successfully compete with a human picker is a monumental task. A skilled human worker picks over a million fruit per season at a rate of 1000 fruit per hour while getting paid approximately one half-cent per fruit [2]. The human picker coordinates visual and tactile senses to locate a fruit, manipulate his arms through the leaves and around limbs to grasp the fruit, and with a twisting-pulling motion, detach the fruit from the tree. Automating this operation, with mechanical manipulators coordinated with vision and/or other sensors, is a challenge undertaken by researchers worldwide.

One of the first published accounts of robotic tree fruit harvesting research was by Parrish and Goskel [3]. A robotic system, consisting of a three-degrees-of-freedom manipulator and global machine vision, was developed to evaluate the technical feasibility of harvesting apples robotically. In this study, a digital image of a fruit tree scene was analyzed to identify any ripe fruit projected in the image. If one was detected, the centroid location of that fruit's projection in the image plane was determined. Based on this centroid location and the relative position between camera and manipulator, a trajectory was calculated and the prismatic third link extended along this trajectory, in a dead reckoning fashion, until fruit contact was sensed with a mechanical touch sensor. Fruit detachment was not attempted since end-effector development was not undertaken.

The simplicity and effectiveness of Parrish and Goskel's basic concept - global machine vision for identification and planar location of ripe fruit and the three-degrees-of-freedom manipulator with terminating prismatic link for harvesting - has been recognized by subsequent researchers in this field. A

robotic tree fruit harvesting system, proposed by the Martin Marietta Corporation [4], followed this philosophy for the design of its individual harvesting modules. The proposed system consisted of three harvesting modules mounted on a flatbed trailer which could be towed through a grove or orchard. Each module would contain an R-R-P harvesting manipulator with a finger type end-effector and global machine vision. Dead reckoning guidance of the harvesting manipulator based on calculated planar fruit locations, determined from the machine vision, was the proposed method for fruit harvesting. Alignment of camera optics with manipulator geometry was suggested to reduce computations involved in determining manipulator trajectories to targeted fruit.

An operational robotic apple harvester has been developed at CEMAGREF (Centre National Du Machinisme Agricole Du Genie Rural, Des Eaux Et Des Forets) Montpellier, France by Grand D'Esnon [5]. Again, many of the same concepts used in the Parrish and Goskel design were shared by this machine. Also, as with the Martin Marietta design, alignment of optics with manipulator was used. The P-R-P harvesting manipulator consists of a hollow tube arm mounted in a vertical frame and a rotating cup end-effector. The hollow tube rotates about an axis skewed slightly from vertical and can translate both in and out and up and down the frame. Attached to the carriage supporting the hollow tube is a CCD line scan camera. While the carriage moves up along the vertical frame, the camera scans successive horizontal strips of a fruit tree scene. When a fruit is detected, the control computer initiates movement of the hollow arm such that it follows the optical path of the light reflected from the fruit to the linear CCD array. Opto-electric sensors incorporated in the end-effector detect proximity with a fruit. When this occurs, forward motion of the arm is stopped and a rotating cup picking mechanism activated to detach the fruit. Once detached, the fruit rolls down the hollow tube arm into a conventional harvest bin. The French apple harvester has operated successfully in the laboratory picking fruit randomly attached to a dark surface covered with branches and leaves. The harvester, requiring no a priori knowledge of fruit positions, could pick an average of 15 fruit per minute.

Common to all three robotic tree fruit harvesting systems is the use of dead reckoning guidance of the manipulator. However, a problem with this harvesting approach is that changes in a fruit's position after it has been targeted by the global vision system can result in an unsuccessful harvest cycle. The inability to adjust to fruit motions during a harvest cycle will greatly degrade the performance of a robotic harvester out in groves and orchards where fruit will be moving due to canopy disturbances from wind and possibly other robots.

In this work, an alternative to the dead-reckoning guidance harvesting concept is developed. The method presented utilizes

real-time two-dimensional fruit location information from a camera in the end-effector for feedback guidance control of a harvesting robot. This vision-servo approach to manipulator guidance provides for the automatic compensation of fruit motions during a harvest cycle and thus, is more compatible with actual grove and orchard conditions.

II. GEOMETRY ANALYSIS

A schematic of an R-R-P tree fruit harvesting robot is shown in Figure 1. The manipulator rotates about intersecting horizontal and vertical axes, Z_0 and Z_1 (joint variables θ_1 and θ_2 respectively). The third, prismatic link slides about axis Z_2 (joint variable d_3) which is always perpendicular with Z_1. A CCD camera is incorporated in the rotating lip picking mechanism such that Z_2 is coincident with the optical axis of the camera.

Let O_c be a coordinate frame for the camera with the Z_c axis coincident with Z_2 and the camera's optical axis (see Figure 2). The camera's image plane is oriented parallel to the X_c, Y_c plane and the geometric center located at (0,0,-f) where f is the focal length of the lens. Let p_c be a vector describing the position of an object in the camera coordinate frame. The position of the object's projection in the image plane is given by [6]:

$$p_i = T_p p_c \qquad (1)$$

where

$$T_p = \begin{bmatrix} -f/z & 0 & 0 & 0 \\ 0 & -f/z & 0 & 0 \\ 0 & 0 & -f/z & 0 \\ 0 & 0 & 0 & 1 \end{bmatrix} \qquad (2)$$

$$p_c = [\, x \quad y \quad z \quad 1 \,]^T \quad \text{and}$$

$$p_i = [\, x_i \quad y_i \quad -f \quad 1 \,]^T.$$

Let O_w be the world coordinate frame with origin at the intersection of axes Z_0, Z_1. The robot, when in the home position ($\theta_1 = \theta_2 = 0$), is oriented such that the (Z_0, Z_1) plane is coplanar with the (Z_w, X_w) plane and Z_2 is coincident with Z_w. A homogeneous transform (see [6]) relating the position and orientation of the camera coordinate frame in O_w to the joint variables is given by:

$$T_3 = \begin{bmatrix} -s_1 & -c_1 c_2 & c_1 s_2 & d_3 c_1 s_2 \\ c_1 & -s_1 c_2 & s_1 s_2 & d_3 s_1 s_2 \\ 0 & s_2 & c_2 & d_3 c_2 \\ 0 & 0 & 0 & 1 \end{bmatrix} \quad (3)$$

where $s_i = \sin\theta_i$, $c_i = \cos\theta_i$, and d_3 is the distance along Z_2 the camera is extended from axis of rotation Z_1. The orientation of O_c can be determined from the upper left 3 x 3 matrix in T_3. Going from left to right, the three column vectors in this orientation matrix defines the directions of the X_c, Y_c, and Z_c axes, respectively. The fourth column vector of T_3 defines the position of O_c. Note that Z_c is always parallel with the position vector.

Let p_w be a vector specifying an fruit's position in world coordinates. For a known position of the manipulator (i.e. θ_1, θ_2, d_3 known), the fruit's position in camera coordinates (p_c) can be obtained with the following equation (see Figure 3):

$$p_c = T_3^{-1} p_w. \quad (4)$$

Substituting the above expression for p_c into (1) we have

$$p_i = T_p T_3^{-1} p_w. \quad (5)$$

Equation 5 relates the position of a fruit's projection in the image plane, p_i, to the position of the manipulator and the position of the fruit in the world coordinate frame. For the vision-servo problem it is important to know how changes in the manipulator's position affect p_i. Specifically, we are interested in obtaining closed form solutions that relate changes in x_i, y_i to changes in θ_1, θ_2, respectively. These relationships are referred to as vision gains and are expressed as:

$$K_{vx} = \frac{dx_i}{d\theta_1}, \quad (6)$$

$$K_{vy} = \frac{dy_i}{d\theta_2}. \quad (7)$$

We begin the derivation for the vision gains by assuming the manipulator is initially aligned with a fruit located at some world coordinates $p_w = [\ x_w \quad y_w \quad z_w \quad 1\ ]^T$ and at a distance z from the camera. The configuration of the manipulator in the aligned position is (θ_1, θ_2, d_3). Since the manipulator and

fruit are aligned, we know that the fruit must lie along Z_c at a radial distance of $(d_3 + z)$ from origin O_w. Thus, p_w can be expressed as:

$$p_w = (d_3 + z)a \qquad (8)$$

where $a = [T_3(1,3) \quad T_3(2,3) \quad T_3(3,3) \quad 1]^T$ (the unit vector obtained from the third column of T_3) and defines the Z_c direction. Substituting (8) into (5) and solving for p_i, we find that $x_i = y_i = 0$ as expected under aligned conditions. Suppose the manipulator is misaligned by rotating axes one and two incremental amounts $d\theta_1$, $d\theta_2$ to a new configuration $(\theta_1+d\theta_1, \theta_2+d\theta_2, d_3)$. Due to this misalignment, the projection of the fruit will offset from the center of the image plane by incremental amounts dx_i, dy_i. Solving equation (5) for these offsets, dropping second order terms in $d\theta_1$, $d\theta_2$ from the solution, and letting $\sin(d\theta_i) = d\theta_i$, $\cos(d\theta_i) = 1$, results in :

$$dx_i = \frac{f(d_3 + z)d\theta_1 s_2}{z} \qquad (9)$$

$$dy_i = \frac{-f(d_3 + z)d\theta_2}{z} . \qquad (10)$$

Solving Equations 9 and 10 for the vision gains results in,

$$K_{vx} = fs_2(d_3/z + 1) \qquad (11)$$

$$K_{vy} = -f(d_3/z + 1). \qquad (12)$$

It is important to note that K_{vx} and K_{vy} are approximately inversely proportional to z and proportional to d_3. Thus, during a harvest cycle as the camera-picking mechanism extends toward a targeted fruit, d_3 increases and z decreases, requiring increasingly smaller adjustments in θ_1 and θ_2 to compensate for robot misalignment. In addition, K_{vx} is proportional to the sine of θ_2. This implies that the further a targeted fruit is off the horizontal (recall that when $\theta_2 = 0$ the manipulator is pointing straight up), increasingly larger adjustments in θ_1 are required to compensate for horizontal misalignment of the robot.

Also important is the fact that the vision-servo problem is decoupled geometrically. That is, changes θ_2 do not affect x_i, and changes in θ_1 do not affect y_i. This can be seen by the absence of a $d\theta_2$ term in (9) and an absence of a $d\theta_1$ term in (10). This geometric decoupling allows us to treat the two dimensional vision-servo problem as two independent one dimensional problems, greatly simplifying the analysis.

III. CONTROL LAW ANALYSIS

A block diagram of a single axis vision-servo feedback loop is shown in Figure 4. Dynamics of the link to be controlled are represented by $G_R(s)$. Input to this block is joint torque, T. Output from the robot block is angular position, θ. Note that for the output of $G_R(s)$ to be angular position and not angular velocity, integration of output is implied. The vision gain is indicated as K_v. Input to this block is angular position of the link being considered (θ_1 or θ_2). Output from this block is p, the pixel coordinate where the centroid of the targeted fruit is projected onto the image plane (x_i or y_i). This centroid pixel is subtracted from p_a, the pixel position corresponding to the geometric center of the image plane. The resulting error signal is acted upon by a feedback control law, G_c, to eliminate the offset with adjustments of joint torque.

This section examines the dynamics of the vision-servo loop, as described above, under proportional and proportional plus derivative control. It is assumed that the pixel coordinates corresponding to the centroid of a targeted fruit's projection are available in real-time (at least 30 hz) and discretization effects on closed-loop dynamics are insignificant. Also, it is assumed that axes one and two are decoupled dynamically as well as geometrically, thus allowing a single-input-single-output treatment of the control problem.

Proportional Control

The dynamics of a rotational manipulator link actuated with an electric servo motor can be approximated by [7]:

$$J\ddot{\theta} + F\dot{\theta} = T \tag{13}$$

where θ is the angular position of the link (θ_1 or θ_2), T the motor torque, J the effective inertia of link, load and actuator, and F a viscous damping factor. For a permanent magnet DC servo motor, a common assumption is that torque is proportional to motor armature current, I. Taking this into account, we have:

$$J\ddot{\theta} + F\dot{\theta} = K_m I \tag{14}$$

where K_m is a motor dependent constant. Motion control of the manipulator link is achieved through an amplifier which controls armature current. For a proportional controlled vision-servo loop, armature current is determined with:

$$I = K_p^*(p_a - p) \tag{15}$$

where K_p^* is the proportional control constant, p_a and p are as defined above. Using the vision gains derived earlier, we can

rewrite (15) in terms of link angular position as:

$$I = K_p^* K_v(\theta_a - \theta) \tag{16}$$

where K_v is the appropriate vision gain for the link being considered, θ_a the angular position of that link corresponding to manipulator - target alignment, and θ the actual link position. Combining K_p^* and K_m into a single proportional controller gain, K_p, and substituting (16) for the right hand side of (14), results in:

$$J\ddot{\theta} + F\dot{\theta} = K_p K_v(\theta_a - \theta). \tag{17}$$

The resulting closed-loop transfer function for the proportional controlled vision-servo problem is:

$$G_{cl}(s) = \frac{w_n^2}{s^2 + 2w_n \zeta s + w_n^2} \tag{18}$$

where

$$w_n = (K_p K_v / J)^{1/2} \tag{19}$$

$$\zeta = F / [2(JK_p K_v)^{1/2}]. \tag{20}$$

From (19) we see that w_n, the natural frequency of the vision-servo loop, is proportional to the square root of the controller gain - vision gain product. From (20) we see that the damping ratio, ζ, is inversely proportional to the square root of this product. Recall from (11) the dependency of K_{vx} on the vertical position of a targeted fruit, the distance the camera is extended, and the object to fruit distance. Likewise from (12), recall the dependency of K_{vy} on d_3 and z. Thus, as K_{vx} and K_{vy} increase during extension phase of a harvest cycle, the natural frequency of the closed-loop system increases and the damping ratio decreases. This can cause the link to oscillate with increasing frequency and magnitude as the camera nears the fruit. However, if d_3, z, and θ_2 are measurable, this effect can be compensated for through adjustments in controller gains according to simple schedules based on (11) and (12). These schedules are:

$$K_{px} = \frac{K_{fpx}(1 + d_{f3}/z_f)}{s_2(1 + d_3/z)} \tag{21}$$

$$K_{py} = \frac{K_{fpy}(1 + d_{f3}/z_f)}{(1 + d_3/z)} \tag{22}$$

where K_{fpx}, K_{fpy} are axis one, axis two vision-servo gains, respectively, obtained from tuning the control loops on a tar-

geted fruit located on the horizontal (i.e. θ_2 is approximately 90 degrees) with the camera a fixed distance d_{f3} out and the fruit a fixed distance z_f from the camera.

A problem with using simple proportional control to vision-servo a manipulator is the inability adjust the closed-loop damping ratio and natural frequency independently. Increasing K_v increases the natural frequency but decreases the damping ratio. Thus, the bandwidth of a vision-servo loop under proportional control will often be limited due to this conflicting coupling of w_n and ζ . To overcome this problem, a Proportional plus Derivative (PD) control law can be used.

Proportional Derivative Control

For a PD controlled vision-servo loop, armature current is determined by:

$$I = K_p^*(p_a - p) + K_d^*(\dot{p}_a - \dot{p}) \qquad (23)$$

where K_d^* is the derivative gain. By combining K_m and K_p^* into a single constant K_p, K_m and K_d^* into a constant K_d, noting that $\dot{p}_a = 0$, and incorporating the vision gain, we can rewrite (14) as:

$$J\ddot{\theta} + F\dot{\theta} = K_p K_v(\theta_a - \theta) + K_d K_v \dot{\theta}. \qquad (24)$$

The resulting closed-loop transfer function for the PD controlled vision-servo loop has identical form as (18) with w_n determined as in (19). However, the expression for the damping ratio is now:

$$\zeta = (F + K_d K_v) / [2(JK_p K_v)^{1/2}]. \qquad (25)$$

From (25) it is seen that K_d can be used to adjust ζ independent of w_n. Thus, PD control provides more flexibility in tuning the vision-servo loop. Theoretically, any combination of w_n and ζ can be achieved through appropriate choices of K_p and K_d. Under PD control, the bandwidth of a vision-servo loop is limited more by the torque driving capability of the actuation device than by the structure of the control law (as was the case with proportional control).

With PD control, changes in K_v during a harvest cycle must be compensated for by appropriate adjustments of both K_p and K_d. The schedules for K_p to accomplish this were presented in (21) and (22). The schedules for K_d are of identical form:

$$K_{dx} = \frac{K_{fdx}(1 + d_{f3}/z_f)}{s_2(1 + d_3/z)} \quad (26)$$

$$K_{dy} = \frac{K_{fdy}(1 + d_{f3}/z_f)}{(1 + d_3/z)} \quad (27)$$

where K_{fdx}, K_{fdy} are derivative gains for axes one and two, respectively, obtained from tuning vision-servo loops under the conditions specified earlier.

PD control is not without its limitations. The derivative control mode makes the vision-servo loop more sensitive to variations in vision measurements of fruit position. This can be particularly troublesome when camera to fruit distances are small and the fruit occupies a large portion of the camera's field of view. Under these conditions, small variations in the reflected light from the fruit (primarily due to variations in lighting conditions and leaf occlusions) can produce large changes in the centroid position of the targeted fruit's projection on the image plane. These changes can result in excessive control (torque) signals, degrading the performance of the PD controlled vision-servo loop. To avoid this problem, the relative contribution of the derivative mode to the control signal must be reduced or eliminated as z decreases.

IV. SYSTEM EVALUATION

Experimental Setup

The performances of the control laws presented in this work were evaluated on a three-axis General Electric GP66 industrial arm. Kinematically, the GP66 and the harvesting manipulator shown in Figure 1 were identical with one exception; a fixed offset between axes Z_1 and Z_2. It was assumed that the effects of this offset were negligible on vision-servo dynamics. Attached to the end of the GP66 was a rotating lip picking mechanism similar to the one shown in Figure 1. A CCD camera with a 6.5 mm focal length lens and strobe lamp were incorporated into the picking mechanism as indicated in Figure 1. A Motorola VME/10 computer was used for manipulator motion control and image processing. A Datacube VVG-128 VME bussed card was used for acquisition, storage, and display of 485v x 384h x 8 bit images. A citrus canopy was simulated in the laboratory using plastic oranges and foliage attached to a wooden frame with stiff wire. The simulated canopy was placed against a black background.

A simple red filter was used to emphasize the contrast between fruit and foliage. High contrast images resulted which were thresholded at an appropriate gray level through a hardware lookup table on the VVG-128 board producing binary images of the tree fruit scene. Similar results have been obtained on scenes of actual fruit and foliage using a narrow bandpass optical filter with passband centered near 680 nm, the chlorophyll absorption band, where the fruit to foliage reflectance ratio is at a maximum.

Simple blob detection and characterization algorithms were developed to process images of fruit tree scenes. At the completion of an image acquisition, a spiral search would be performed to detect the blob closest to the image center. If one was detected, the blob's horizontal and vertical diameters and position of its centroid were determined. If the diameters were less than the minimum projected by a fruit within picking range, the spiraling search would continue, searching for the next blob. If the detected blob satisfied the diameter criteria, it would be classified as a target fruit and a picking cycle initiated. Once a fruit was targeted, detection and characterization algorithms would be executed on successive images starting the spiral search where the targeted fruit's centroid was located in the previous image. Image processing algorithms provided x_i, y_i values and horizontal diameter data to the vision-servo control routine at standard television frame rates (30 hz). The horizontal diameter data was used to estimate camera to fruit distance, z, since all plastic fruit were of the same size.

Proportional Control Law Evaluation

Initially, fixed gain vision-servo control loops for axes one and two were tuned holding d_3 and z constant. The robot was positioned at $\theta_1 = 0$, $\theta_2 = 90$ degrees, and $d_3 = 1200$ mm and a target fruit suspended 600 mm in front of the camera along the Z_c axis. Next, θ_1 and θ_2 were moved to offset the fruit's projection from the center of the image array by approximately -90 pixels vertically and horizontally. Axes one and two were vision-servoed until the fruit's projection returned to the center of the image array (horizontal pixel 190, vertical pixel 244). The procedure was repeated several times, varying K_{px} and K_{py}. From this tuning procedure, values for K_{px} of -20 and K_{py} of -20 were selected.

A scheduled gain control law was implemented according to equations (21) and (22) using values for K_{fpx}, K_{fpy}, d_{f3}, and z_f obtained from the fixed gain tuning procedure. Due to the range of θ_2 on the GP66 manipulator of only +/- 30 degrees from the horizontal, the s_2 term in Equation (21) was omitted from this implementation. In Figure 5 the performance of a scheduled gain control law for axis one is compared to that of a fixed gain control law during a typical harvest cycle. Initially, the target

fruit was horizontally offset from the center of the image by approximately 100 pixels and located 600 mm from the camera. For evaluation purposes, a precise measurement of camera to fruit distance was obtained manually. As soon as the projection of the fruit was detected in the image plane, axis three was extended and axes one and two vision-servoed centering the fruit. Both the fixed gain and scheduled gain control laws provided adequate control until the camera was approximately 250 mm from the fruit. At this point, the vision-servo loop under fixed gain control began to oscillate. As the camera approached the fruit, a substantial increase in the magnitude of these oscillations was evident. Vision-servoing with a scheduled gain controller maintained adequate picking alignment throughout the harvest cycle.

PD Control Law Evaluation

A procedure, similar to the one described above, was used to evaluate the performance of the vision-servo loop under PD control. Little improvement in the response of the vision-servo loop was obtained with PD control. Upon examining the output of the PD algorithm when K_{dx} and K_{dy} were of moderate magnitudes, it was found that the control signals were saturating, driving axis one and two servo motors to their limits. Due to this, the effects of the derivative control mode were not fully realized and the performance PD control could not be properly evaluated.

V. CONCLUSIONS

The robotic system described in this work, vision-servoed by the scheduled gain proportional control law, has been used to successfully harvest tree fruit from a simulated canopy. A maintained harvesting cycle time of four seconds has been achieved. The vision-servo control system provides the harvesting robot with the capability to track fruit motions during a harvest cycle.

A single arm system is being designed specifically for tree-fruit harvesting and will incorporate many refinements over the current laboratory harvester described in this paper. Some of the refinements are: 1) color machine vision, 2) adaptive vision-servoing and 3) collision detection techniques. A computer simulation package is being developed to aid in the design and analysis of the grove harvester. The field harvester will provide researchers with a portable test-bed to evaluate robotic tree-fruit harvesting technology under actual grove conditions. Upon completion and satisfactory evaluation of the grove harvester, the basic building block of a multiple arm tree fruit harvesting robot will have been developed. It is expected that the single arm system will be in the grove within the next two years.

Acknowledgments

The authors wish to thank the Florida Department of Citrus, Lakeland, Odetics Inc., Anahiem and the R. J. Reynolds Corporation, Winston-Salem for their financial support of this research.

References

1. Martin, P. L., Labor-intensive agriculture, Scientific American, vol. 249 no. 4, pp. 54-59. 1983.

2. Coppock, G.E., Robotic principles in the selective harvest of Valencia Oranges, in Proc. of the first intl conf on robotics and intelligent machines in agriculture, published by ASAE, St. Joseph, Mi, pp. 138-145, 1984.

3. Parrish, E. A., and A. K. Goskel, Pictorial pattern recognition applied to fruit harvesting, Trans. ASAE 20(5), pp. 822-827, 1977.

4. Tutle, E. G., Image controlled robotics in agricultural environments, in Proc. of the first intl conf on robotics and intelligent machines in agriculture, published by ASAE, St. Joseph, Mi, pp. 84-95, 1984.

5. Grand D'Esnon, A., Robotic harvesting of apples, in Proc. of Agri-Mation I, published by ASAE and SME, St. Joseph, Mi., pp. 210-214. 1985.

6. Paul, R. P., Robot manipulators: mathematics, programming, and control, MIT Press, Cambridge, Mass., 279 pp., 1981.

7. Synder, W. E., Industrial robots: computer interfacing and control, Prentice-Hall, Englewood Cliffs, NJ., 325 pp., 1985.

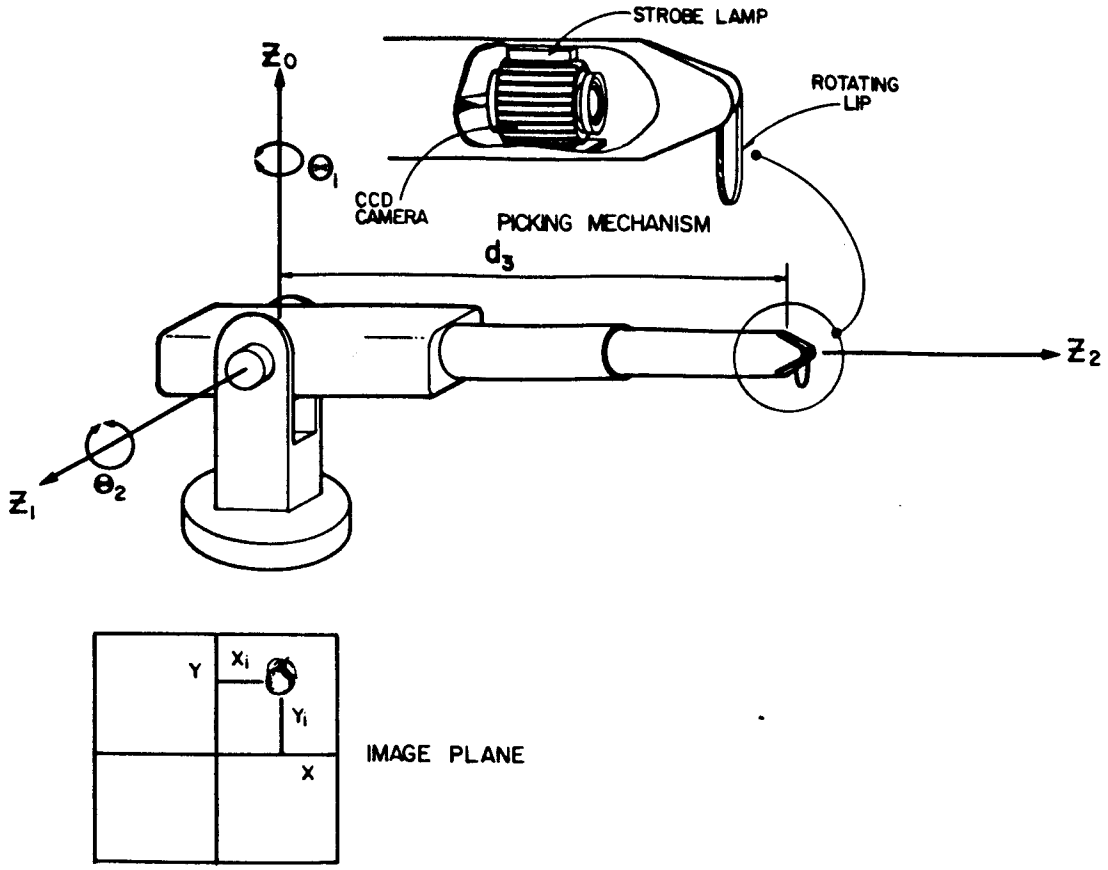

Figure 1. An R-R-P tree fruit harvesting robot.

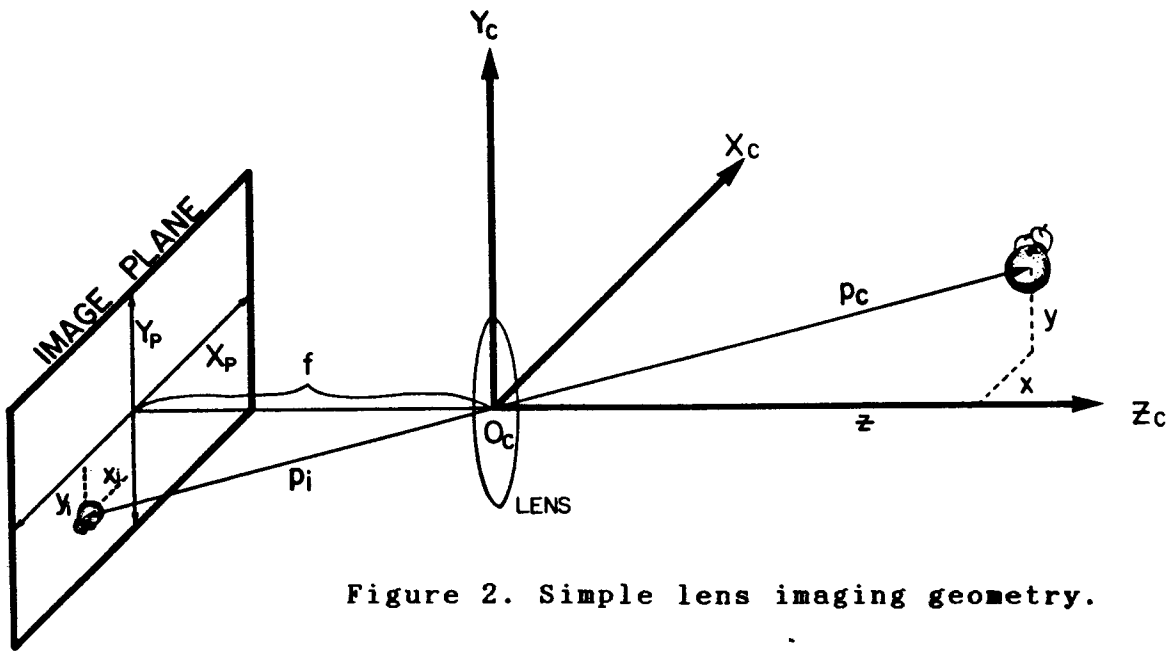

Figure 2. Simple lens imaging geometry.

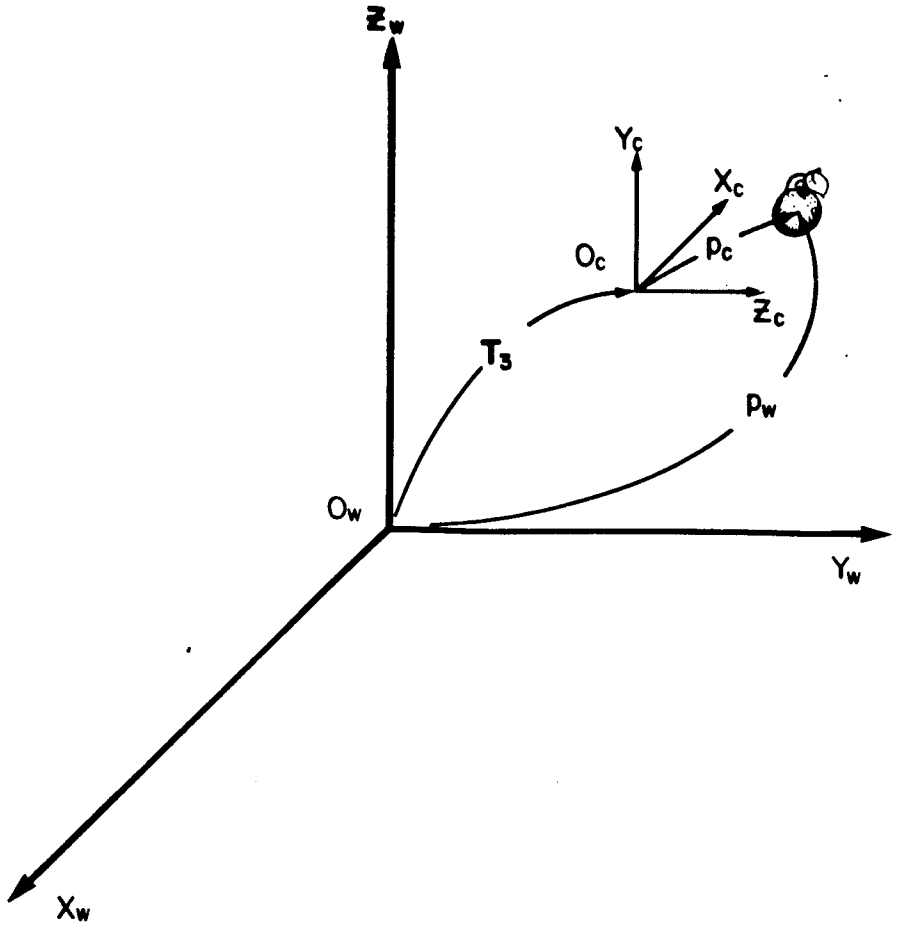

Figure 3. Object - coordinate frames relationship.

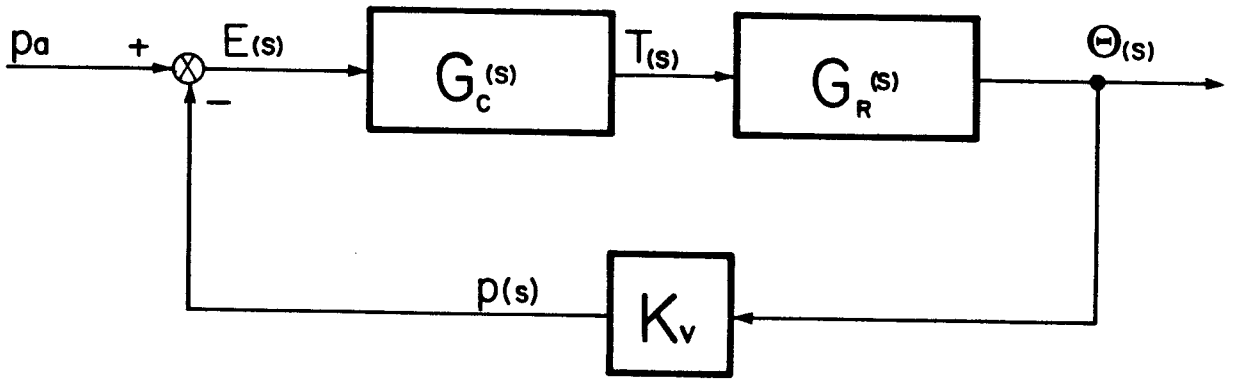

Figure 4. Vision-servo loop block diagram.

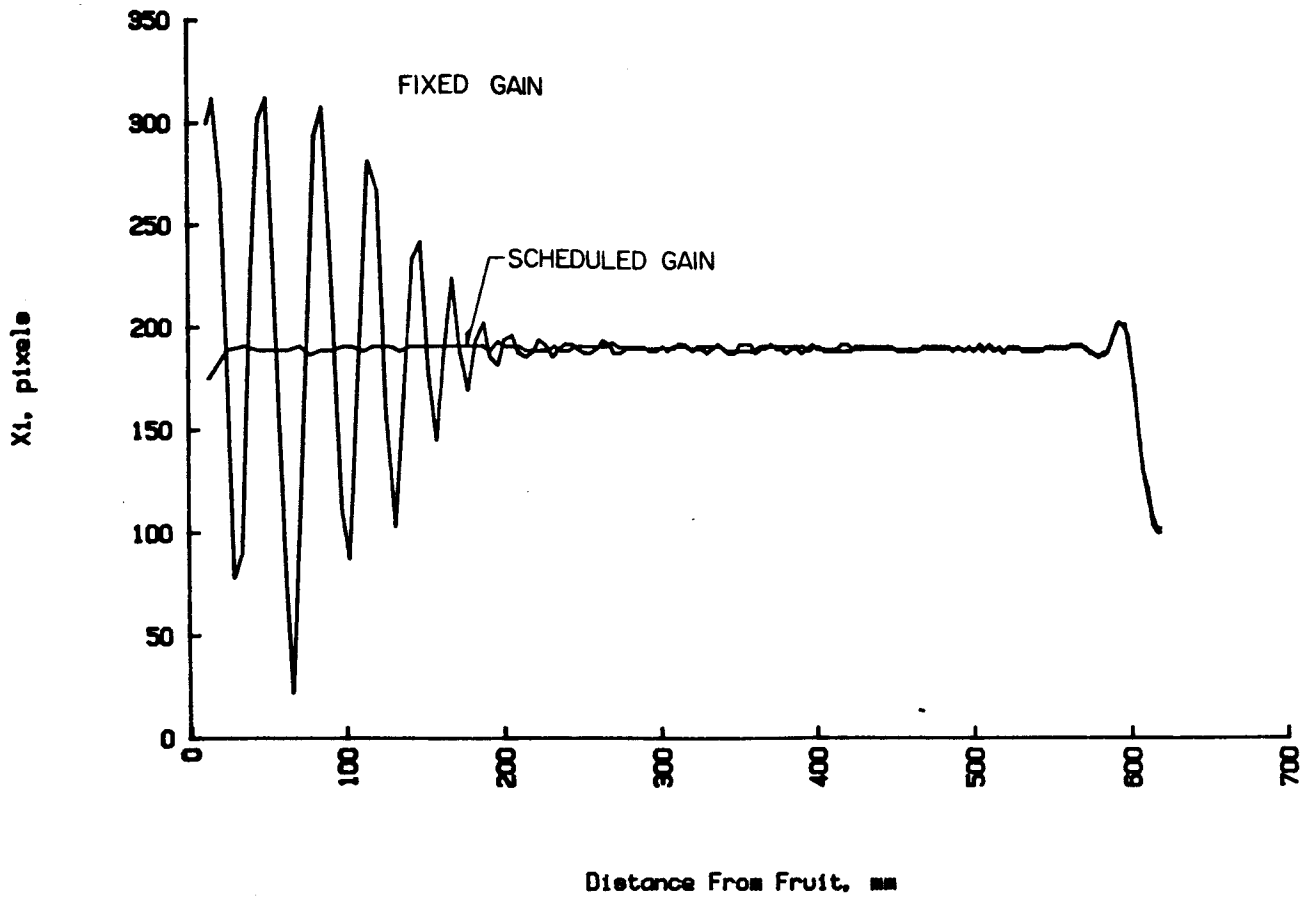

Figure 5. Performance comparison of fixed gain and scheduled gain proportional control laws for axis one.